

# On the melting behaviour of calcium monoxide under different atmospheres: A laser heating study

D. Manara <sup>a,\*</sup>, R. Böhler <sup>a,c</sup>, L. Capriotti <sup>a,b</sup>, A. Quaini <sup>a,b,1</sup>, Z. Bao <sup>a</sup>, K. Boboridis <sup>a</sup>,  
L. Luzzi <sup>b</sup>, A. Janssen <sup>a</sup>, P. Pöml <sup>a</sup>, R. Eloirdi <sup>a</sup>, R.J.M. Konings <sup>a,c</sup>

<sup>a</sup> European Commission, Joint Research Centre, Institute for Transuranium Elements (ITU), P.O. Box 2340, 76125 Karlsruhe, Germany

<sup>b</sup> Politecnico di Milano, Department of Energy, “Enrico Fermi” Center for Nuclear Studies, via Ponzio 34/3, 20133 Milan, Italy

<sup>c</sup> Faculty of Applied Sciences, Delft University of Technology, Mekelweg 15, 2629 JB Delft, The Netherlands

Received 8 July 2013; received in revised form 6 December 2013; accepted 10 December 2013

Available online 3 January 2014

## 1. Introduction

The main goal of the present work is the reassessment of the melting point of CaO and its dependence on the environmental conditions. Known for centuries as a geological material and a disinfectant, CaO (also called calcia or burnt-lime) is a common alkaline-earth oxide with fcc NaCl crystal structure.<sup>1</sup> CaO is produced by dissociation of CaCO<sub>3</sub> upon heating, according to the well known equilibrium<sup>1</sup>:



Equilibrium (1) is easily reversible at room temperature, which makes CaO relatively unstable in contact with the CO<sub>2</sub> of the air. Reaction (1) occurs whenever lime-based minerals are brought to high temperature. Knowledge about the

high-temperature behaviour of calcia is therefore paramount for the study of number of these minerals under extreme conditions, especially in relation to their mechanical stability, optical properties and equation of state.<sup>2,3</sup>

On the other hand, very numerous applications justify the great technological interest of CaO, that make its chemical industry production second only to that of H<sub>2</sub>SO<sub>4</sub>.<sup>1</sup> Broadly employed in the chemical and construction industries, it can also be used as a source of heat when put in contact with water: an exothermal reaction occurs with a production of calcium hydroxide. Furthermore, recent studies on Inert Matrix Nuclear Fuel (IMF)<sup>4,5</sup> suggest calcia also as a stabilising element for this innovative anti-proliferation nuclear fuel.

An especially interesting property is that it can withstand temperatures above 1800 K without dissociating or melting that is, it can be considered as a refractory material.

### 1.1. The controversial melting point of CaO

The melting/freezing point of CaO is certainly higher than all the International Temperature Scale 1990 (ITS90) established

\* Corresponding author. Tel.: +49 7247 951 129.

E-mail address: [dario.manara@ec.europa.eu](mailto:dario.manara@ec.europa.eu) (D. Manara).

<sup>1</sup> Current address: CEA Saclay, DEN/DANS/DPC/SCP/LM2T, 91191 Gif-sur-Yvette Cedex, France.

Table 1  
CaO melting temperatures reported in the literature.

$T_m$ (K)	Reference	Experimental approach
2863	Noguchi et al. (1966) <sup>8</sup>	Solar furnace (uncertain)
2890	Panek (1979) <sup>9</sup>	Electrical furnace
2833	Shevchenko (1979) <sup>10</sup>	Electrical furnace
3223	Foex (1966) <sup>11</sup>	Solar furnace
2886	Hlaváč (1982) <sup>12</sup>	Electrical furnace
3178	Yamada (1985) <sup>7</sup>	Solar furnace
3200	NIST JANAF	REVIEW
3222	This work	Laser heating

references.<sup>6</sup> It had even been studied as a new higher temperature standard reference,<sup>7</sup> save for the obvious large discrepancy in the available experimental data. The existing values for the melting temperature of CaO vary between 2833 K and 3223 K<sup>7–12</sup> (Table 1). Lower melting temperatures were generally obtained with traditional crucible heating techniques. With the sole exception of the solar furnace heating experiments performed by Noguchi et al.<sup>8</sup>, where the clear thermal arrest observed above 3100 K was arbitrarily attributed to a liquid/gas transition rather than a solid/liquid one, experimental methods in which the contact between burnt lime samples and their containment was limited systematically yielded higher values. This observation led Foex<sup>11</sup> and Yamada<sup>7</sup> to the conclusion that the reported “lower” melting/solidification temperatures did not correspond to pure CaO, but rather to compositions that largely reacted with their containment. Consequently, the high melting/freezing point measured by these latter Authors has been retained in the JANAF Tables,<sup>13</sup> which report for CaO ( $3200 \pm 50$ ) K. If the 1986 study by Yamada et al.<sup>7</sup> is the latest experimental work available, further discussion on the calcia melting behaviour can be found in more recent literature about phase diagram studies of the Ca–O system<sup>14</sup> or thermodynamic optimisation (CALPHAD) of systems including CaO as an end member.<sup>15–24</sup> In particular, Pelton et al.<sup>15,16</sup> criticised the high melting point of burnt lime reported in the JANAF tables, noticing the good agreement between data reported at lower temperature, and the fact that a lower melting point would be thermodynamically more consistent with phase equilibria assessed for multi-component systems including CaO. In this interpretation, the higher-temperature phase transition reported by Foex<sup>11</sup> and Yamada<sup>7</sup> was attributed to CaO boiling rather than melting. More authors<sup>14,17–19</sup> recently accepted the viewpoint of Pelton et al., whereas others<sup>20–24</sup> used in their phase diagram assessment the JANAF data. The reasons of the existing discrepancies and controversy can be understood in the light of the complex high temperature behaviour of calcia, from both an optical and chemical viewpoints.

## 1.2. Optical properties

CaO exhibits a particular optical behaviour when it is heated beyond a temperature ranging between 2000 K and 2200 K. It then emits a dazzling bright white light called limelight or Drummond light, known since the beginning of the 19th Century,<sup>26–27</sup> and already largely used in high-power light sources, film projection and illuminating devices without any physical explanation

of the involved phenomena. The most recent assessment of this subject is due to Kubarev,<sup>27</sup> who experimentally observed a rather abrupt evolution of calcium oxide from an optically hardly absorbing body to an almost ideal black body in a temperature range from 2000 K to 2300 K (see Appendix I). Materials with this behaviour can be called “semitransparent”, although the term is probably somewhat misleading. The optical phenomenon is in fact more precisely related to a “low-absorptivity”–“high absorptivity” transition. The material can be either highly transparent or highly reflective, depending of the photon energy, in its “low absorptivity” state. When the critical temperature identified by Kubarev<sup>27</sup> was reached, the emissivity  $\varepsilon_\lambda$  (equal to the absorbivity within the validity of Kirchhoff’s law)<sup>25</sup> of calcium oxide increased by a factor of about 10, which implied a complete change of the whole optical behaviour of this material. Considering  $\varepsilon_\lambda \approx 1$  at high temperature, Kubarev obtained a reasonable value of 0.1 at low temperature, which was in agreement with emissivity values found for other “white” oxides.

The only possible technique to measure phase transitions at  $T > 2500$  K is optical pyrometry, based on the detection of the sample thermal radiance. Optical pyrometers measure the “radiance temperature”  $T_\lambda$ , which can only be converted into real temperature  $T$  if the sample’s emissivity  $\varepsilon_\lambda$  is known, as indicated by Eq. (2)<sup>25</sup>:

$$\frac{1}{T} = \frac{1}{T_\lambda} + \frac{\lambda}{c_2} \cdot \ln \varepsilon_\lambda \quad (2)$$

where a value of  $14,388 \mu\text{m K}$  is used<sup>25</sup> for the fundamental constant  $c_2$  (cf. Appendix I). It can therefore be understood how a sudden change in emissivity makes it particularly difficult to measure stable thermograms on a calcia specimen heated beyond the melting point, unless the sample itself is either contained in another black-body shaped material (with, however, a high contamination risk), or shaped itself as a black body cavity (which however induces a large uncertainty due shape loss upon melting). The first approach was adopted in research based on crucible furnace heating,<sup>9,10</sup> the latter by Yamada et al.<sup>7</sup>, Noguchi et al.<sup>8</sup> and Foex<sup>11</sup> who employed a solar furnace heating technique. In the current work, the sample surface is directly measured in parallel to the sample emissivity, which allows an *in situ* determination of the sample real temperature.

Further details about radiance emission of a hot sample are given in Appendix I.

## 1.3. Chemical properties

The most fundamental high-temperature chemical property of calcia for the present study is the solubility of oxygen in liquid Ca. Calcium is well known to exist only as a pure metal or a divalent cation. Nonetheless, Bevan and Richardson<sup>28</sup> estimated that above the Ca + CaO eutectic temperature ( $1107 \text{ K} \pm 1.5 \text{ K}$ ), liquid calcium can dissolve oxygen up to an oxygen atomic fraction  $x(\text{O}) = 0.13\text{--}0.15$  at 1523 K, whereas the solubility experimentally observed by Zaitsev and Mogutnov<sup>18</sup> at temperatures closer to Ca boiling (approximately 1800 K) are of the order of  $x(\text{O}) = 0.10$ . No experimental information is available beyond such temperature range up to the melting point of CaO.

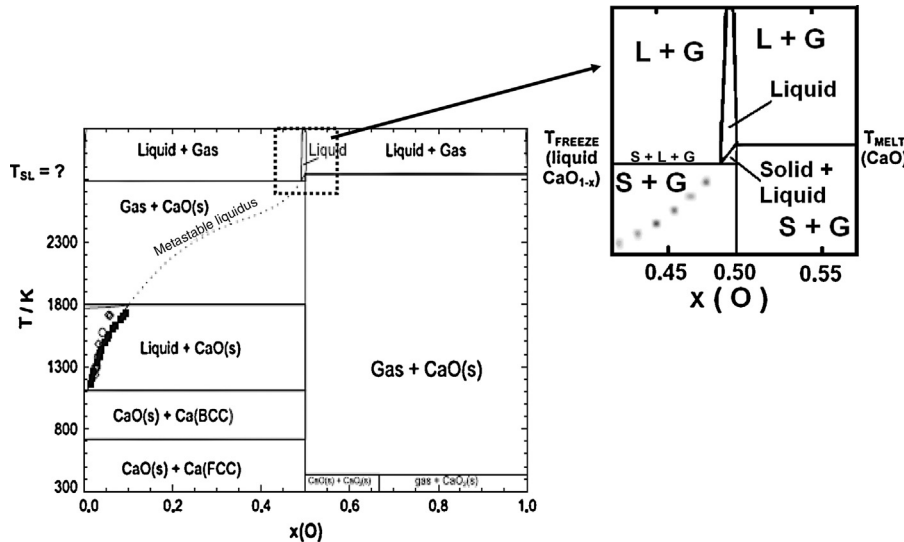


Fig. 1. The Ca–O binary phase diagram at 1 atmosphere (after the thermodynamic optimisation by Lindberg and Chartrand)<sup>19</sup>. The solid/liquid transition temperature ( $T_{SL}$ ) is still controversial. To be noted, in the inset, that the extrapolated phase boundaries are consistent with the existence of a slightly hypostoichiometric liquid, freezing at the invariant temperature where solid and liquid CaO are in equilibrium with gaseous Ca ( $S + L + G$  line in the inset graph). This invariant temperature is slightly lower than the congruent CaO melting point.

Recently, the thermodynamic calculations of Lindberg and Chartrand<sup>19</sup> showed that the mentioned liquidus line, representing the solubility of oxygen in liquid calcium at equilibrium with CaO, can be prolonged at temperatures higher than the boiling point of Ca, in the hypothesis that the formation of gas is suppressed. This “metastable liquidus”, which can be observed, for example, by suitably increasing the ambient pressure and/or by performing very fast heating/quenching cycles, extends until the CaO melting point. On the other hand, it is commonly accepted<sup>19</sup> that even in equilibrium with atmospheric pressure liquid CaO dissolves more excess calcium than excess oxygen, i.e. it exists on a narrow composition range extending from approximately  $x(O)=0.48$  to  $x(O)=0.5$  (Fig. 1). The corresponding phase boundaries are therefore consistent with the existence of slightly hypostoichiometric liquid, freezing at the invariant temperature where solid and liquid CaO are in equilibrium with gaseous Ca ( $S + L + G$  line in the inset graph). This invariant temperature is slightly lower than the congruent CaO melting point. The chemical behaviour of calcium oxide in the proximity of the congruent melting point becomes, under such conditions, less simple than one would expect for a line compound. For example, the existence of “hypostoichiometric” liquid CaO can open new questions: the effective congruent melting and freezing composition of this compound, the possibility to quench to lower temperature a defective solid starting from the melt, the behaviour of CaO in mixed systems with other oxides, metals or more general compounds, the vapour equilibria under different atmospheres etc.

In the present research, the melting behaviour of calcia is studied under different atmospheres. It is experimentally demonstrated that only under highly oxidising conditions (oxygen, air, compressed air) is the melting/solidification point of this compound reproducible with an acceptable accuracy. Under other atmospheres (inert, vacuum, highly reducing), the observed melting point decreases by an often irregular extent.

## 2. Materials and methods

### 2.1. Sample preparation

Starting material for the current analysis was commercial Alfa Aesar® 99.998% CaO powder. The impurity level was therefore considered to have a negligible effect on the melting behaviour studied in this work, at least within the uncertainty limits of the current approach.

In order to remove  $\text{CaCO}_3$  possibly formed in contact with atmospheric  $\text{CO}_2$ , the powder was heat treated at 1800 K in an Ar flux. Successively, it was cold-pressed into cylindrical pellets of 8 mm in diameter and 2–4 mm thick. The resulting pellets were sintered at 1800 K in an argon flux for 8 h. Samples were then stored under inert atmosphere (dry argon or primary vacuum) until their melting/freezing point measurements.

### 2.2. Very high temperature heating cycles

CaO samples were mounted in a controlled-atmosphere cell closed by a gas-proof quartz window 10 mm thick. Physical contact to their mount was limited by using three or four radially arranged graphite screws to hold them in place. Problems such as vast sample vaporisation and interaction with its containment, typically encountered at high temperatures, were greatly reduced or completely ruled out thanks to the high measurement speed and its containerless character. It was moreover possible to study the effect, on the observed phase transitions, of the gas nature and pressure (up to 0.3 MPa) inside the experimental cell.

The specimens were studied at very high temperature by laser heating combined with fast pyrometry (Fig. 2)<sup>29</sup>. The heating agent was a Nd:YAG 4.5 kW cw laser radiating at 1064.5 nm, programmable with a complex power/time profile. The laser beam, conveyed by fibre optics, impinged on an approximately

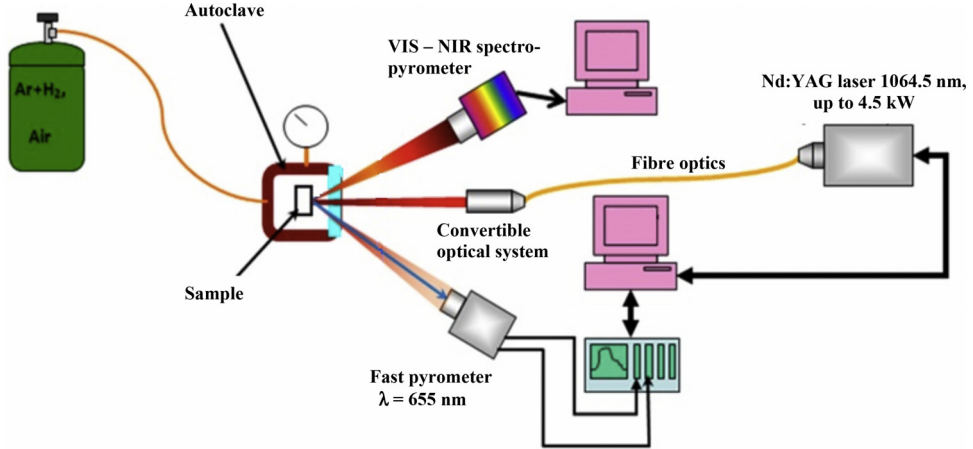


Fig. 2. The experimental set-up used in the current research for laser heating CaO under controlled atmosphere.

circular area of 8 mm in diameter on the vertical sample surface. Such geometry was chosen in order to minimise interference between the possible formation of a vapour plume from the hot surface and the optical measurement of temperature. The sample surface was heated beyond melting for variable time durations (from a few tens ms to a few seconds). This time scale was short enough for the liquid mass to be held in place by the surface tension. The corresponding depth of the molten pool varied from a few  $\mu\text{m}$  to about 100  $\mu\text{m}$ . The invariance of the recorded phase transition temperatures with the dwelling time in the liquid state could thus be checked, to study possible segregation or non-congruent vaporisation phenomena. The sample was let cool naturally at the end of the high power laser pulse. Cycles of three successive heating pulses beyond melting were performed in each experiment. In between them, the sample could be alternatively cooled to room temperature, or kept at an intermediate temperature, higher than the “semitransparent” transition temperature assumed to be approximately 2150 K, by irradiating it with the same laser but at a lower power. The second situation was preferred because it allowed a better mechanical stability of the sample throughout repeated shots, and therefore to an improved result reproducibility over successive shots. In fact, the material absorvity sudden increase easily causes an uncontrollable temperature excursion more than a thousand K above the melting point (see Fig. 4), accompanied by massive vaporisation and cracking of the sample. Preheating the sample at a temperature around the “semitransparent” transition allowed a better control of the material behaviour throughout the heating cycles. This could be obtained by irradiating the specimen with a constant laser beam power of 100 W, delivering a surface power density of approximately  $200 \text{ W cm}^{-2}$ . Higher power pulses, reaching up to  $1000 \text{ W cm}^{-2}$  (depending on the pulse duration) were then sent to the specimen in order to heat it beyond melting. Finite element simulations of the heating cycles,<sup>30</sup> supported by micro-imaging of the quenched samples, ensured that at the beginning of the cooling process homogeneous temperature was produced in the laser irradiated area for a depth of a few tens  $\mu\text{m}$ . Thermal analysis was then performed on the “natural” cooling stage of the cycle.

### 2.3. Temperature measurements

The sample temperature was measured on a spot of 0.5 mm in diameter at the centre of the laser-heated area by means of a pyrometer equipped with a fast logarithmic amplifier (settling time of about  $10 \mu\text{s}$  to 1% of log output) and operating at 655 nm.<sup>29</sup> It was calibrated against a standard tungsten-ribbon lamp in the range of 1800–2500 K, ensuring traceability to the International Temperature Scale of 1990.<sup>31,32</sup> The calibration was linearly extrapolated beyond this temperature, and its validity, as well as the quality of the optical windows and the alignment, were tested by measuring *in situ* the melting radiance temperatures of molybdenum and tungsten (2530 K and 3207 K, respectively, at 653 nm)<sup>6</sup>.

For the measurement of the normal spectral emissivity NSE ( $\varepsilon_\lambda$  in Eq. (2)), a further spectro-pyrometer, based on a linear array of 256 Si photodiodes, was used to record the sample thermal radiance in the range of 488–1011 nm. This instrument allows a more complete spectral analysis, whereby its main disadvantage is in the poorer time resolution (one spectrum per millisecond at best)<sup>29</sup>. Due to low signal-to-noise ratio, moreover, only the range 550–920 nm was useful for the current measurements. A photodiode operating at 649 nm was calibrated up to 2500 K using the tungsten-ribbon lamp and this calibration was transferred to a tubular-cavity variable-temperature graphite blackbody-furnace up to 3300 K. The remaining photodiodes were then calibrated with this blackbody, allowing a conversion of output signal to spectral radiance over the entire useful wavelength range. The measured radiance spectra recorded on calcia in the vicinity of the melting/solidification point were fitted by least-squares regression to Planck’s distribution law for blackbody radiance, modified by a wavelength- and temperature-dependent function assumed to represent the normal spectral emissivity. Although such an approach is known to be affected by low numerical accuracy,<sup>33</sup> compared to other techniques, it can be considered as acceptable for high emissivity materials, like calcia at high temperature, which are known to follow a grey body (GB) behaviour (NSE quasi-independent of  $\lambda$ ). Such a behaviour has been confirmed with the present measurements, yielding for freezing CaO in air

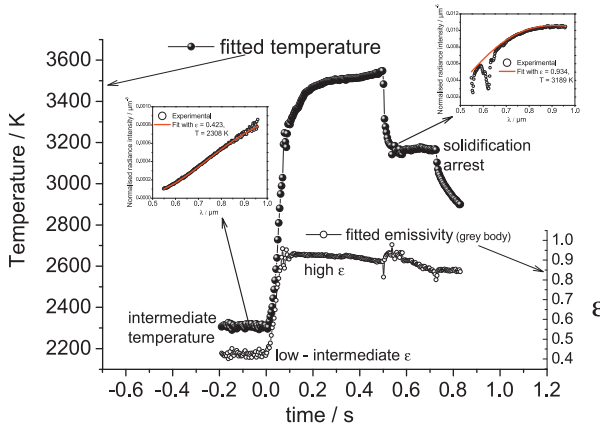


Fig. 3. Application of the current radiance spectral analysis procedure to a thermogram recorded during a laser heating pulse on a CaO sample under argon. Each full circle of the reported thermogram (temperature- vs.-time curve) represents the temperature giving, together with the corresponding emissivity value (open circle in the emissivity-vs.-time curve), the best fit for the radiance spectrum recorded at a given time, with an accumulation time of 4 milliseconds per spectrum. The two insets show examples of radiance spectra recorded one at an intermediate temperature of approximately 2300 K (slightly above the “low-absorptivity”–“high absorptivity” transition) and one at the beginning of the solidification thermal arrest. Analytical curves fitting the experimental spectra are shown, too. One such spectrum was recorded and fitted per each experimental point (circle) displayed.

$\varepsilon_{GB} = 0.92 \pm 0.05$  for  $0.655 \mu\text{m} \leq \lambda \leq 0.92 \mu\text{m}$ , in agreement with previous data<sup>27</sup> and recent ab-initio calculations of CaO optical properties.<sup>34</sup>

Fig. 3 shows an example application of this procedure to a thermogram recorded during a laser heating pulse on a CaO sample under argon. Each full circle of the reported thermogram (temperature- vs.-time curve) represents the temperature giving, together with the corresponding emissivity value (open circle in the emissivity-vs.-time curve), the best fit for the radiance spectrum recorded at a given time. An accumulation time of 4 milliseconds per spectrum was set in this particular example. The two insets show examples of radiance spectra recorded one at an intermediate temperature of approximately 2300 K (slightly above the “low-absorptivity”–“high absorptivity” transition) and one at the beginning of the solidification thermal arrest. Analytical curves fitting the experimental spectra are shown, too. The broad absorption bands observed in the high-temperature radiance spectra were not considered in the fitting procedure, and are extensively discussed further in this paper. A clear transition in the emissivity is observed, in fair agreement with the data reported by Kubarev.<sup>27</sup> However, it should be noted that the lower emissivity values are possibly affected by unquantifiable uncertainty due to parasite laser radiation reflected into the spectro-pyrometer (see further Section 3.1). Most important for the current study was the high-emissivity value ( $0.92 \pm 0.05$ ), characteristic of CaO at temperatures close to melting and beyond. This emissivity value has been used to transform radiance into real temperature through Eq. (1) in pyrometer-recorded thermograms around the melting transition. More mathematical details about emissivity analysis are given in Appendix I.

## 2.4. Post-melting sample characterisation

Number of experimental methods was used to characterise calcia samples after the laser heating/melting/freezing cycles. Melted specimens were recovered for post-melting analysis by scanning electron microscopy (SEM, JSM-5610, JEOL®, Tokyo, Japan) and energy-dispersive X-ray spectroscopy (EDX). Cross-sections through melted surfaces were prepared for microstructural analysis and imaged unetched. Higher-magnification transmission electron microscopy (TEM) images of the melted/refrozen material were also taken thanks to a TECNAI® microscope.

Raman spectra were recorded by means of a Jobin-Yvon® T64000 confocal spectrometer with notch filters and single grating (mono configuration). This system is equipped with a microscope for confocal micro-Raman measurements. Spectra were acquired with a Peltier cooled CCD matrix, with a resolution of  $1 \text{ cm}^{-1}$ . A 488 nm Ar<sup>+</sup> laser was used as impinging light source, with a power, on the sample surface, variable between 0.1 mW and 10 mW. Spectra were recorded with a  $0^\circ$  geometry (on the reflected beam).

X-ray diffraction (XRD) was performed in this work using a Bruker® D8 Advance diffractometer (Cu-K $\alpha$ 1 radiation) with a  $2\theta$  range of  $10\text{--}120^\circ$  using  $0.009^\circ$  steps with 2 s of count time per step at operating conditions of 40 kV–40 mA. The XRD instrument was equipped with a LynxEye®  $3^\circ$  linear position sensitive detector. TOPAS 4.2 software was used for Rietveld refinement of the experimental XRD pattern.

X-ray photoelectron spectroscopy (XPS) was used to study the oxidation state of the final material, quenched from temperatures close to melting. All XPS spectra were recorded using a Mg K $\alpha$  excitation radiation at 1253.6 eV in an UHV chamber with a background pressure of about  $5 \times 10^{-10}$  mbar. The instrument used in this case was the Omicron® EA-125 hemispherical deflection analyser with a resolution of 0.5 eV. The system was calibrated using the Au-4f<sub>7/2</sub> of a sputter-cleaned polycrystalline AU standard set to a binding energy (BE) of 84.0 eV. The kinetic energy of photoelectrons (PE) were analysed at constant analyser energy scan mode with a pass energy of 20 eV. The detailed scans were performed at medium magnification mode with an angular acceptance of  $\pm 4^\circ$ . The area analysed with this configuration is 3 mm in diameter.

## 2.5. Uncertainty analysis

The most significant uncertainty sources have been combined, according to the independent error propagation law,<sup>29</sup> to yield relative uncertainty bands corresponding to one standard deviation (1-k coverage factor). These uncertainty sources concern the current temperature scale definition  $\delta T$  (i.e. the uncertainty in the pyrometer calibration), the NSE assessment  $\delta T_{\varepsilon\lambda}$  and the experimental data dispersion ( $1-\sigma$  standard deviation) on the current phase transition radiance temperature data  $\delta T_{\lambda,m}$ , this latter being the main source of uncertainty:

$$\delta T_m = \sqrt{\delta T^2 + \delta T_{\varepsilon\lambda}^2 + \delta T_{\lambda,m}^2}. \quad (3)$$

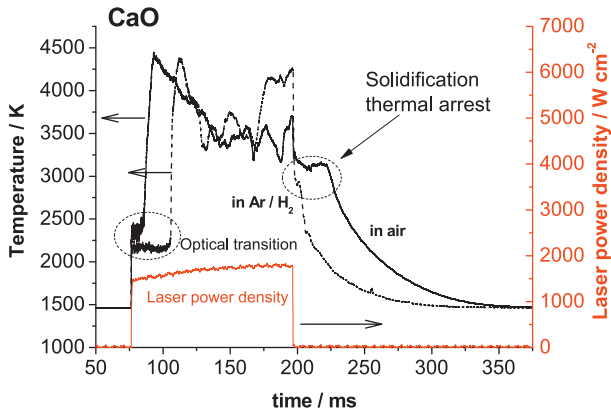


Fig. 4. Typical thermograms recorded on CaO in air and in Ar + 6% H<sub>2</sub> at 0.655 μm. Effects of the absorption bands (see Fig. 6) have been taken into account by correcting the emissivity used to obtain the true temperature curves. To be noted the optical transition around 2150 K on the heating stage, where CaO transforms from mostly reflecting (low emissivity) to a highly absorbing (high emissivity), and the irregular features of the thermogram when the sample is fired to very high temperature.

The high relative uncertainty bands reported in the next section should not surprise when one considers the extreme conditions under which the current data have been measured, and the factors potentially affecting the radiance measurements. In particular, one can assume that the main uncertainty causes are here the sample surface morphology, the onset of vaporisation and surface sputtering and the possible metastable supercooling of liquid below the equilibrium freezing temperature. These phenomena can be minimised by setting a suitable pressure and atmosphere in the sample-holding vessel, and by properly choosing the laser power–time profile.

### 3. Results

#### 3.1. Heating–cooling cycles

Fig. 4 shows two thermograms measured on a CaO sample under compressed air or argon + 6% hydrogen (both at 0.3 MPa) with a single high-power (close to 1500 W cm<sup>-2</sup>) heating pulse conceived to overcome the low absorbivity-high absorbivity limit for this material. The dynamics of melting and freezing under the current conditions can be figured out by interpreting the recorded thermogram with the help of heat and mass transport simulations of the same kind of processes reported in previous publications.<sup>30,35</sup> A first apparent thermal arrest can be observed on heating at a radiance temperature around 2150 K. This corresponds to the mentioned low absorbivity-high absorbivity optical transition. More precisely, the observed behaviour here seems to be consistent with a high reflectivity–high absorbivity transition, at least at the near-infrared laser wavelength. It is actually obvious from the thermogram shape, that CaO mostly reflects the impinging laser radiation at temperatures lower than the optical transition point. In fact, the thermogram shape reproduces, in the first part of the experiment, the shape of the heating laser power profile. Some of the laser radiation is then certainly reflected into the pyrometer

which detects it as parasite radiation, probably too intense to be properly filtered by the pyrometer’s optical path. It can be clearly seen from the thermogram, that after the sample has absorbed enough energy to overcome such optical transition, its temperature starts to increase very rapidly, reaching almost 4500 K in a few milliseconds. Because of the conditions far from the thermal equilibrium in this stage of the experiment, the possible crack formation and interaction between the laser beam fraction reflected into the pyrometer detector and the thermal radiation emitted by the sample, features on the heating flanks of the thermogram were generally ignored for the present analysis. Even a thermal arrest corresponding to melting was only very seldom observed under the current conditions. In fact, the uncontrollable formation of cracks on the surface and the massive vaporisation (the boiling point – probably corresponding to a slight inflection sometimes observed around 3450 K – was certainly overcome) were likely to play a major role in the entire heating process, and particularly on the very irregular features of the thermogram after the maximum temperature was reached. Nonetheless, the very high maximum temperature was still moderate enough for the sample to remain integral throughout the experiment. It was therefore possible to clearly identify the freezing thermal arrests on the cooling flanks of the thermogram. There, also some super-cooling can be seen. This phenomenon has to be ascribed to the high cooling rate, which hinders the crystal nucleation in liquid calcium oxide. Solidification starts at the bottom of the molten pool formed on the sample surface, where the solid interface fosters growth of solid inside the liquid cooled below the equilibrium freezing temperature. Only when the growing solid reaches the upper, free liquid surface (the one seen by the pyrometer), the recorded temperature starts to rise until the equilibrium freezing temperature is reached.

As mentioned in Section 2.2, an alternative approach to the melting/freezing cycles consisted in keeping the sample at an intermediate temperature, higher than the “semitransparent” transition temperature, by irradiating it with a lower power of the laser beam between two high-power pulses. It was observed that such an approach gave a better stability of the sample throughout repeated shots. Fig. 5 reports three successive thermograms recorded under the latter conditions. Their shape is more “ordinary”, with neither sudden heating to extremely high temperature, nor irregular features during the sample dwelling beyond melting. Under these conditions, the melting/freezing arrests were observed at slightly higher temperature, and their repeatability was largely improved, too. It can also be noticed in Fig. 5 that during the high-power laser pulses the sample surface temperature tended to plateau at an almost constant value depending on the experimental conditions. Such a value was systematically different for the samples heated under air (around 3600 K) and those heated under argon-hydrogen (around 3450 K). This behaviour can probably be related to the onset of boiling in the two different experimental conditions, although such assumption should be confirmed by further research.

The set of data obtained with the second approach was obviously more suitable for any statistical analysis. However, data obtained with single laser pulses followed by natural

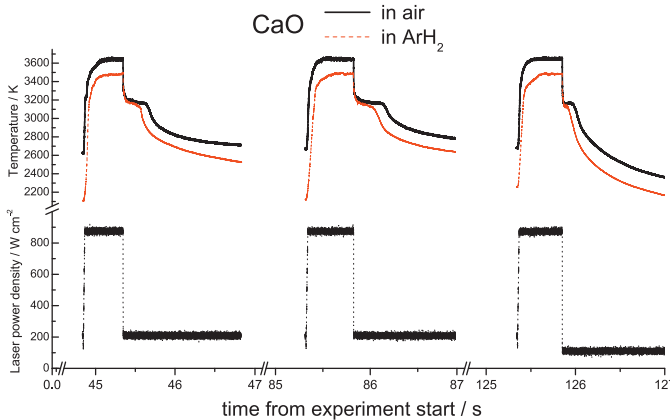


Fig. 5. A sequence of three laser heating pulses performed on CaO in air and in Ar + 6% H<sub>2</sub> at 0.655 μm. Effects of the absorption bands (see Fig. 6) have been taken into account by correcting the emissivity used to obtain the true temperature curves. The heating laser power was maintained at 50 W cm<sup>-2</sup> in between the high-power pulses. In this way, the sample (solid or resolidified) was not allowed to cool below the optical transition point.

cooling to room temperature were somewhat instructive, in that they showed that the observed solidification points were lower under those “poorly-controlled” conditions.

### 3.2. Radiance measurements

If very high-temperature radiance measurements are generally awkward due to the extreme conditions, in calcia the situation is even more complicated because of the well-known existence of F and F<sup>+</sup>-centre luminescence.<sup>36–43</sup> Such a phenomenon is related to the fact that photon irradiation of calcia samples excites emission and absorption bands due to photo-electronic transitions in oxygen vacancies with one (F<sup>+</sup>) or two (F) free electrons, mostly detectable in the UV-vis range.<sup>42</sup> Radiance spectra recorded on liquid and solidifying CaO under oxidising and reducing atmospheres are shown in Fig. 6. Because beyond the semitransparent threshold the emissivity of calcia is very close to 1,<sup>27</sup> these spectra are very close to Planck’ black-body spectra at the solid/liquid transition temperature. However, clear absorption bands can be observed in the visible range.

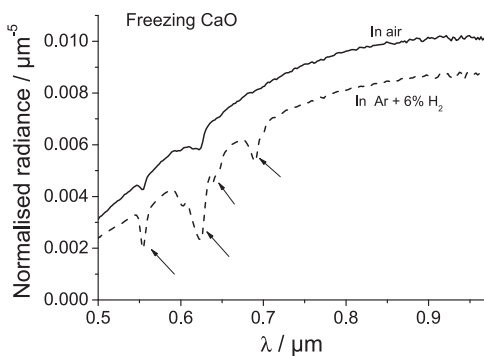


Fig. 6. Radiance (Planck) spectra of solidifying CaO in air (solid line) and in Ar + 6% H<sub>2</sub> (dashed line). Absorption bands are clearly visible between 0.55 μm and 0.7 μm, more intense and numerous in the sample heated in Ar/H<sub>2</sub>, where they correspond to the creation of oxygen defect-related colour centres and darkening of the material.

These bands are more numerous and intense for samples melted under a reducing atmosphere, which agrees well with the darker colour displayed by such samples after the heating cycles (see Fig. 6). From a pyrometric viewpoint, it would therefore be preferable to measure the radiance of calcia away from spectral windows affected by these absorption bands, in order to avoid unpredictable emissivity excursions. It is important to remark that an absorption peak is visible just around 0.65 μm, a wavelength typically used in radiance thermometry, only in samples heated under a reducing atmosphere.

### 3.3. Melting/freezing behaviour under different atmospheres

Several experiments were repeated on different CaO samples under different atmospheric conditions and with different laser pulse shapes. The vessel was filled with either compressed air or argon in order to operate under an oxidising or reducing atmosphere, respectively. In general, the observed solidification temperatures were reproducible within the reported uncertainty bands, those measured under a reducing atmosphere (3192 K ± 40 K) being slightly, but systematically lower and more uncertain than those measured under air (3222 K ± 25 K) (Fig. 7). For samples melted under a reducing atmosphere, thermograms measured by the spectro-pyrometer in the near-infrared range (750 nm ≤ λ ≤ 900 nm) were used in the statistics together with those recorded at 0.65 μm in order to rule out the risk of unquantifiable effects of emissivity variations due to the onset of the absorption bands displayed in Fig. 6. For the same reason, thermograms recorded by the fast pyrometer at 0.655 μm from CaO solidifying in Ar/H<sub>2</sub> were corrected (cf. Eq. (2)) with ε<sub>λ</sub> = 0.85 (instead of ε<sub>λ</sub> = 0.95 used in the other cases).

When the sample was heated under an oxidising atmosphere, the detected melting temperatures resulted comparable with those measured by Yamada et al.<sup>7</sup> Since also the latter authors performed their melting/freezing cycles under air (at atmospheric pressure, 0.1 MPa), it is reasonable to conclude that under these conditions, stoichiometric CaO was most probably stabilised and maintained throughout the heating cycle, and a congruent melting transition was observed. It is also worth noticing that the fair agreement between the current thermal arrests, recorded under compressed air at 0.3 MPa, and those observed by Yamada at atmospheric pressure corroborates their attribution to solidification rather than boiling. One would in fact expect a much more evident dependence of a boiling point on the external pressure, whereas the melting/solidification point variation due to a change on the external pressure of a few tenths of a MPa should be negligible.<sup>3</sup>

A further inflection was occasionally detected at higher temperature (around 3450 K) only in thermograms recorded under a reducing atmosphere (Ar + 6% H<sub>2</sub> at 0.3 MPa). These inflections, reported in Fig. 7, have been tentatively assigned to CaO boiling/condensation under a reducing atmosphere. Such attribution would be in fair agreement with the observation, mentioned above, that in laser pulse series the temperature tended to be stabilised around 3450 K under pressurised argon + 6% hydrogen (Fig. 5).

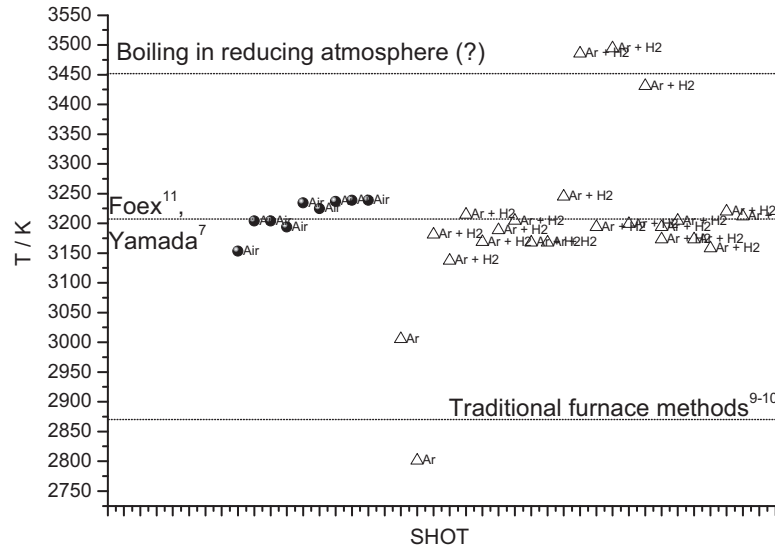


Fig. 7. The current solidification point data of CaO compared with literature results. Further inflections occasionally observed at higher temperature and possibly attributable to boiling/condensation in reducing conditions are also reported.

The solidification arrest observed in samples melted under a reducing atmosphere was only in a couple of cases comparable with the set of lower melting/freezing data reported in the literature,<sup>8–10</sup> these cases always corresponding to single laser pulses, and not series of shots between which the sample was kept at an intermediate temperature above 2000 K. In the vast majority of the current experiments, the solid/liquid transition was observed at a higher temperature. Under reducing atmosphere, it was slightly (a few tens Kelvin), but systematically lower than that measured under air and affected by a considerably poorer reproducibility. It is possible, therefore, that liquid calcia samples were more sensitive, under these latter conditions, to reduction in contact with the experimental atmosphere, leading, upon solidification, to the formation of a solid richer in oxygen defects. Correspondingly, the resulting colour of such refrozen material is dark grey–black as opposed to the bright white obtained in the case of CaO melted and re-solidified under air (Fig. 8a and b). The kinetics and effectiveness of such a reduction would largely depend on the sample surface morphology and the experimental parameters (laser beam intensity, atmosphere, heating duration etc.), explaining the poor reproducibility.

#### 4. Discussion

The current experimental results show that the melting/solidification (and, probably, boiling) behaviour of calcium oxide is influenced by the atmosphere in which the solid/liquid transition occurs. The maximum transition temperature slightly higher than 3200 K can be consistently reproduced only under strongly oxidising conditions. In this case, also the original colour of calcia (bright white) is maintained throughout the heating/cooling cycle. Under reducing conditions, instead, the refrozen material results considerably darkened with respect to the fresh one (cf. Fig. 8). This latter phenomenon can be attributed to the formation of more colour centres (F or F<sup>+</sup> centres) related to oxygen defects in the re-solidified oxide. Correspondingly, although absorption bands are always observed in CaO at very high temperature, more of them, and with a higher intensity, can be seen in the material heated beyond melting under reducing conditions (cf. Fig. 6). The corresponding liquid solidifies at a slightly lower and less reproducible temperature. In particular, the presence of additional absorption bands in the darkened material close to 0.650 μm and 0.710 μm can be attributed to slight temperature-dependent evolutions of F<sup>+</sup>



Fig. 8. Photos of CaO samples laser melted and refrozen in air (a) and in Ar + 6% H<sub>2</sub> (b).

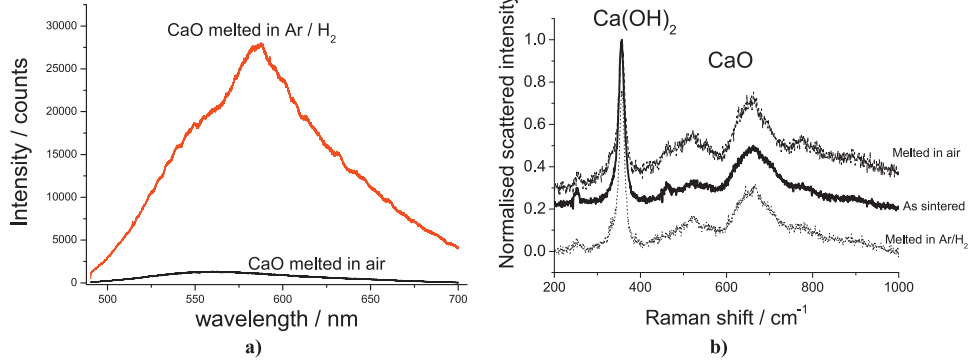


Fig. 9. (a) Room temperature luminescence spectra recorded on the current calcia samples melted and refrozen in air and Ar/H<sub>2</sub> by using the 0.488 μm line of an Ar<sup>+</sup> laser to excite the luminescence, and a Jobin Yvon (R) T64000 Raman spectrometer to detect it. (b) Raman spectra of calcia samples studied in the present research with the same laser source.

centre modes already reported elsewhere.<sup>42,43</sup> The temperature dependence of such modes has already been addressed in earlier publications, although never at temperatures close to CaO melting.<sup>38,40</sup>

In addition, room temperature luminescence spectra have been recorded on the current calcia samples melted and refrozen in air and Ar/H<sub>2</sub> by using the 0.488 μm line of an Ar<sup>+</sup> laser to excite the luminescence, and a Raman spectrometer to detect it (in a similar way as in Ref. 39). Such luminescence spectra showed that only the broad and intense absorption band attributed to the 3T<sub>1u</sub> → 1A<sub>1g</sub> transition around 0.585 μm<sup>39–43</sup> was clearly visible in “darkened” samples melted in a reducing atmosphere, with an evident shoulder detectable around 0.550 μm. The last feature corresponds to the only weak and very broad band visible in the luminescence spectrum of calcia heated under air (Fig. 9a). This characterisation is consistent with the formation of oxygen defects in calcia melted and refrozen in a reducing atmosphere, similarly to other irradiation techniques (laser, neutrons, electrons) employed for the creation of colour centres. Leaving for another paper a more detailed analysis of such colour centres at high temperature, here it is essential to remark that there seems to be a relation between their formation, possible oxygen losses and the melting behaviour (cf. the inset in Fig. 1).

On the other hand, no significant differences can be appreciated in the Raman spectra of the same samples (Fig. 9b). Characteristic bands<sup>44</sup> due to a Raman-active combination of transversal optical and acoustic phonons around 530 cm<sup>-1</sup> and the transversal optical phonon at 655 cm<sup>-1</sup> are visible in all cases, confirming that the onset of oxygen defects has no direct effect on the vibrational modes of CaO. It can also be noted that in all samples a clear Raman peak at 363 cm<sup>-1</sup> shows that the surface is contaminated with Ca(OH)<sub>2</sub><sup>45</sup> as a result of the prompt reaction with humidity at room temperature. However, calcium hydroxide decomposes<sup>46</sup> at around 700 K, ensuring that such contamination had no effect on the current melting behaviour study.

The formation of colour centres is mostly related to the existence of Frenkel and Schottky defects in the CaO crystal,<sup>43</sup> with therefore hardly any influence on the overall composition of the

material. Such a behaviour can be related to the phase boundaries extrapolated by Lindberg and Chartrand<sup>19</sup> concerning the equilibria between oxygen-defective liquid calcia, solid CaO and gaseous Ca (here reported in Fig. 1), where it is shown that the presence of oxygen defects thermodynamically stabilises liquid CaO at temperatures lower than that of congruent melting. The current experimental observations would be in fair qualitative agreement with those high-temperature phase boundaries but for the actual values of the invariant temperature at which CaO melts congruently (3222 K ± 25 K in the current assessment) and that of coexistence between solid CaO, liquid CaO<sub>1-x</sub> and gaseous Ca (3192 K ± 40 K).

The inset of Fig. 1 is updated in Fig. 10 with the invariant temperatures assessed in the present research. The determination of the oxygen content x(O) corresponding to the invariant eutectic point denoted as “A” in Fig. 9 still constitutes an open challenge, which could not be resolved by the additional post-melting material characterisation performed in the present research. Calcia samples melted and refrozen both under oxidising and reducing conditions have been studied by Raman spectroscopy, XPS, XRD and transmission electron microscopy. The main results of such characterisation are compared in Figs. 11–13. XRD showed the formation of non-negligible traces of Ca(OH)<sub>2</sub> on the darkened sample surface. This observation is consistent with the fact that a more abundant oxygen defect concentration catalyses

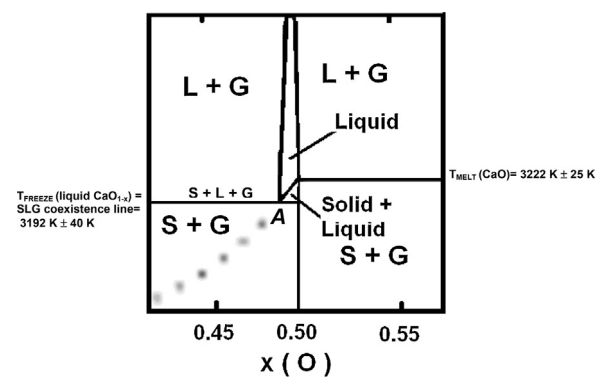


Fig. 10. Tentative phase boundaries of the Ca–O system in the vicinity of the congruent CaO melting point according to the present investigation.

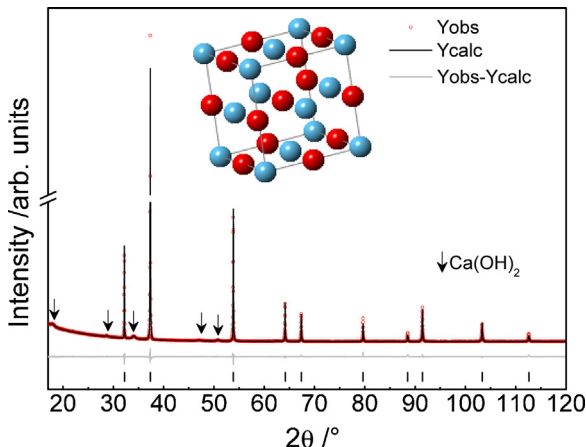


Fig. 11. X-ray diffraction patterns of CaO samples laser melted and refrozen in Ar + 6% H<sub>2</sub> compared to the well known XRD peaks of burnt lime (vertical straight lines – faced centred cubic, space group Fm $\bar{3}$ m,  $a = 0.481056$  (2) nm). No clear differences are detectable, with the exception of broad peaks consistent with the formation of Ca(OH)<sub>2</sub> traces (estimated to a maximum of 5 wt%) on the sample surface (hexagonal, space group P $\bar{3}$ m1,  $a = 0.35912$  (10) nm,  $c = 0.49171$  (2) nm).  $Y_{\text{obs}}$  = observed experimental data;  $Y_{\text{calc}}$  = fitted XRD pattern;  $Y_{\text{obs}} - Y_{\text{calc}}$  = residuals.

prompt reaction of CaO with even small traces of humidity. However, none of the employed techniques showed consistent differences between the two types of samples attributable to the formation of metallic calcium or to different oxygen contents.

To summarise, the current experiments seem to confirm, from a slightly different viewpoint, the conclusions already drawn by Foex<sup>11</sup> and Yamada<sup>7</sup>: stoichiometric liquid CaO freezes congruently at around 3200 K under an oxidising atmosphere and nearly container-less conditions. This also confirms the melting/freezing point reported in the JANAF Tables.<sup>13</sup> Moreover, the current investigation shows in a straightforward fashion that the melting behaviour of calcium oxide is not only dependent on the eventual interaction between sample and its containment, as it was concluded by Foex<sup>11</sup> and Yamada,<sup>7</sup> but also on the atmosphere in which the heating/cooling cycles are carried out under quasi-container-less conditions. As an additional remark, this implies that the attribution of the observed thermal arrests to a liquid/vapour transition, rather than a solid/liquid one, seems unlikely, due to its negligible dependence on the external pressure.

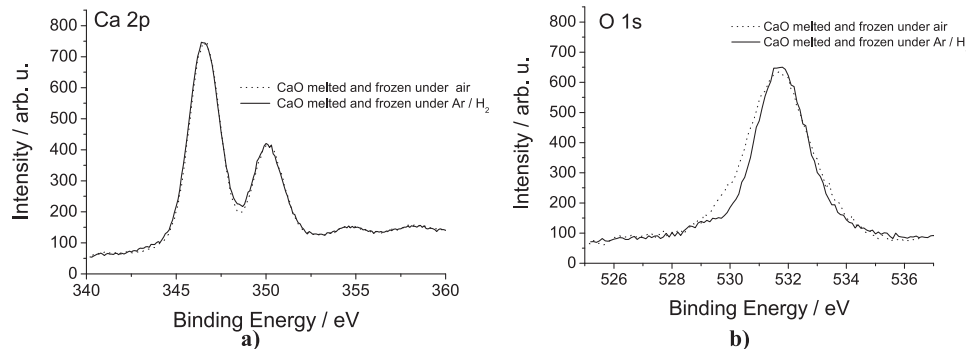


Fig. 12. X-ray photo-electron spectra (XPS) of Ca 3p (a) and O 2s (b) in CaO samples laser melted and refrozen in air (dotted curves) and in Ar + 6% H<sub>2</sub> (dashed curves). No clear differences are detectable following the formation of colour centres in CaO, nor signs of any possible formation of metallic Ca.

In the light of the current results, calcium oxide displays a very high temperature behaviour somewhat similar to that of other oxides, such as MgO, CeO<sub>2</sub>, UO<sub>2</sub>, PuO<sub>2</sub>, NpO<sub>2</sub>, which have been assessed in the last decade.<sup>30,35,47–49</sup>

One could imagine also for calcium oxide under very high temperature and pressure a situation similar to that reported by Ronchi et al.<sup>50</sup> for the equation of state of UO<sub>2</sub>: the definition of a liquid/vapour equilibrium under extreme conditions is not reducible, even in a first approximation, to a single line, but rather to a closed curve with different branches corresponding to boiling and saturation conditions, limited by a critical point.

The current remarks can also have a certain impact on the assessment of pseudo-binary and multi-nary phase diagrams in which CaO constitutes one end member.<sup>15–24</sup> The analysis of some of these systems seems better compatible with a lower melting/freezing point of CaO.<sup>15,16</sup> However, this is in obvious contradiction with the results of the present and other detailed studies performed on the behaviour of pure calcia, results that can be considered to be well established after the current investigation. Such an apparent paradox can be overcome by considering that calcia is most probably richer in defects in such multi-nary phase diagrams in the vicinity of the solid/liquid transition. In fact, the formation of defects and colour centres, resulting in a lower melting/freezing point, is most likely fostered in a mixture of calcia with other oxides or metals. As an example, a similar behaviour was experimentally reported by Foex<sup>11</sup> for the case of SrO, whose melting/solidification point was reduced by over 400 K when measured in a solid solution with just 10 mol% of WO<sub>3</sub>. Still, further systematic research is certainly needed on the solid/liquid equilibria of CaO mixed with small amounts of other oxides or metals in order to fully understand the large difference between the high- and low-melting points reported in the literature for pure calcia. These kinds of systems should be analysed taking into account the existence of defective, or even hypo-stoichiometric calcia at very high temperature. Thus supposedly pseudo-binary systems including CaO as one end member and another metal oxide as the other end member should be better studied in the full ternary diagram calcium-metal-oxygen. This reproduces a situation similar to the one recently assessed for the ternary U–Pu–O system, where the pseudo-binary plane UO<sub>2</sub>–PuO<sub>2</sub> is not sufficient for a complete description of the condensed phase behaviour at temperatures around the melting transition.<sup>51,52</sup>

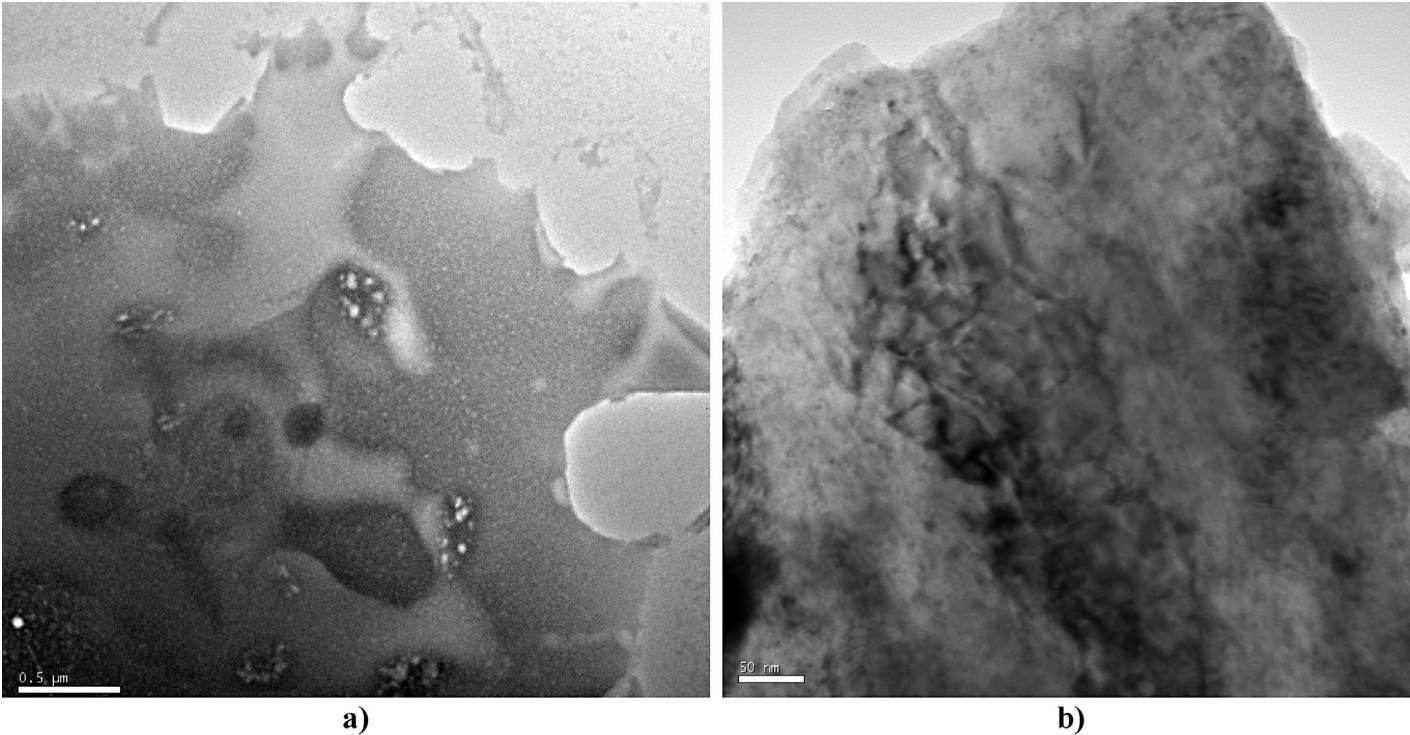


Fig. 13. Transmission electron microscopy (TEM) images of CaO melted and refrozen in Ar + 6% H<sub>2</sub>. No signs of the formation of metallic Ca or defective CaO are detectable.

## 5. Conclusions

In the present work, the melting/freezing behaviour of calcium oxide has been studied by laser heating and fast pyrometry under controlled atmosphere. The influence of the atmospheric conditions on this controversial solid/liquid transition has thus been dealt with for the first time, at least in the authors' knowledge. Despite the complex optical behaviour of calcia at increasing temperature, the current research has yielded consistent results that can be summarised in the following conclusions:

CaO melts congruently around 3200 K (3222 K  $\pm$  25 K according to the present data) under strongly oxidising conditions (air at atmospheric pressure or compressed up to 0.3 MPa).

Under a reducing atmosphere, the solid/liquid transition occurs in calcia at a lower, poorly reproducible temperature at 3192 K  $\pm$  40 K.

Although defects have been detected in both cases in the material at high temperature, they are more numerous and their absorption effects more intense in samples heated and cooled under a reducing atmosphere. Such samples even display a much darker colour after the melting/freezing cycle, attributable to the formation of oxygen-defect-related colour centres in the re-solidified material.

The formation of defects in calcia at high temperature, particularly under reducing conditions, leads to a thermodynamic stabilisation of the liquid up to lower temperatures and, consequently, to a depression of the melting/solidification point. This aspect cannot be ignored in the optimisation of pseudo-binary and multi-nary phase diagrams including CaO as one of the end members, particularly in mixed systems where the formation of oxygen defects can be chemically or physically fostered.

This last point, in particular, has already been raised for other metal–oxygen systems, and should encourage further research in order to fully explain the large discrepancies existing in the literature data on the melting behaviour of CaO, and understand the complex high-temperature behaviour of refractory oxides in general. Besides a deep comprehension of the safety performance limits of refractory oxides in several technological applications, such a research field has a potentially high impact in many different disciplines where these compounds are exposed to high temperatures and extreme conditions. For example, data about calcium monoxide melting have a fundamental importance in understanding the high temperature behaviour of lime-based minerals. Moreover, the present spectroscopic observation of burnt lime optical properties under different conditions will be useful in the study of rocks and gases containing this compound, and, possibly, also in the determination of the nature of their chemical environment.

## Acknowledgements

The authors wish to acknowledge J. Somers, P. Lajarge, P. Coulard and A. Rodrigues (JRC – ITU) for their help in the sample preparation, and P. Raison, D. Bykov and D. Bouexière (JRC – ITU) for their help in the XRD analysis.

## Appendix I. Radiance properties

A material at temperature  $T$  (in K) exchanges with the surrounding environment a spectral radiance  $L_{\lambda bb}$ .<sup>25</sup> For a blackbody (defined as an ideal absorber and an ideal emitter) at the thermodynamic equilibrium  $L_{\lambda bb}$  obeys Planck's law at any wavelength  $\lambda$ :

$$L_{\lambda bb}(T) = \frac{c_{1L}}{n^2 \cdot \lambda^5} \cdot \left[ \exp\left(\frac{c_2}{n \cdot \lambda \cdot T}\right) - 1 \right]^{-1} \quad (\text{A1})$$

where  $c_{1L} = 2hc_0^2$  is the first radiation constant and  $c_2 = hc_0k_B$  is the second radiation constant.  $c_0$  is the speed of light in vacuum,  $h$  Planck's constant, and  $k_B$  Boltzmann's constant. For the purposes of the present work, the index of refraction is always taken to be equal to 1 (being the current medium air or an inert gas close to atmospheric pressure).

For a real body, the radiance intensity exchanged (absorbed or emitted) is related to that of a blackbody at the same temperature by the sample emissivity  $\varepsilon$ . This latter is equivalent, at the thermodynamic equilibrium, to the absorbivity  $a$ , according to Kirchhoff's theorem. At a fixed wavelength spectral absorbivity  $a_\lambda$  and spectral emissivity  $\varepsilon_\lambda$  are used instead of the total parameters. Since pyrometers in the present work are always set up near normal to the sample surface, the angle dependence of  $\varepsilon_\lambda$  is not considered and, 'emissivity' always refers to normal spectral emissivity (NSE). The radiative intensity emitted by a real body of emissivity  $\varepsilon_\lambda$  is compared to that of an ideal blackbody at the same temperature through the following identities:

$$L_\lambda = \varepsilon_\lambda \cdot L_{\lambda bb} = \frac{1}{\lambda^5} \cdot \frac{\varepsilon_\lambda}{e^{c_2/\lambda T} - 1} = \frac{1}{\lambda^5} \cdot \frac{1}{e^{c_2/\lambda T_\lambda} - 1} \quad (\text{A2})$$

$T_\lambda$ , called the radiance temperature, is the temperature at which a perfect blackbody source would emit the same thermal radiation as the sample under investigation at a given wavelength  $\lambda$ . It is therefore a function of the real sample temperature  $T$ , emissivity  $\varepsilon_\lambda$  and the wavelength.

Since the following relation holds ( $\tau_\lambda$  being the sample transmissivity and  $\rho_\lambda$  its reflectivity)

$$\varepsilon_\lambda + \tau_\lambda + \rho_\lambda = 1 \quad (\text{A3})$$

a low-emissivity (low-absorbivity) material is not necessarily only "transparent" but can also be "reflective" at the wavelength of interest.

A material whose  $\varepsilon_\lambda$  is independent of the wavelength is called a grey body (GB). Such behaviour is in general more common to insulators, like calcia and many other oxides, than it is to metallic materials.

In the current research, experimental  $L_\lambda$  curves are fitted by a non-linear parametric function of the type reported in Eq. (A2). The free parameters are the emissivity  $\varepsilon_\lambda$  (which can in turn depend on more parameters) and the real temperature  $T$ . In the case of melting and freezing CaO,  $\exp(c_2/\lambda T) \gg 1$ , and Wien's approximation to Planck's law can be applied,<sup>25</sup> resulting in Eq. (2) of Section 1.2:

$$\frac{1}{T_\lambda} = \frac{1}{T} - \frac{\lambda}{c_2} \cdot \ln \varepsilon_\lambda \quad (\text{A4})$$

According to this simpler equation, the “regular” (close to GB) behaviour of the emissivity of CaO at high temperature can thus be visually checked by plotting the inverse experimental radiance temperature data vs. wavelength. It is then obvious that a GB behaviour will correspond to an increasing straight line in the resulting graph (because  $\varepsilon_\lambda \leq 1$ ), and the NSE will be closer to 1 (black body behaviour), the smaller the slope of the curve. Such a “visual” approach has been used in the current research in order to cross-check radiance data and compensate for the already mentioned poor numerical stability of the emissivity analysis.<sup>33</sup>

## References

- Greenwood NN, Earnshaw A. *Chemistry of the elements*. Cambridge: Pergamon Press; 1994.
- Boslough MB, Ahrens TJ. Shock temperatures in CaO. *J Geophys Res* 1984;**89**:7845–51.
- Sun XW, Song T, Chu YD, Liu ZJ, Zhang ZR, Chen QF. The high-pressure melting curve of CaO. *Solid State Commun* 2010;**150**:1785–8.
- Hellwig Ch, Streit M, Blair P, Tverberg T, Klaasen FC, Schram RPC, et al. Inert matrix fuel behaviour in test irradiations. *J Nucl Mater* 2006;**352**:291–9.
- Lombardi C, Luzzi L, Padovani E, Vetraino F. Thoria and inert matrix fuels for a sustainable nuclear power. *Prog Nucl Energy* 2008;**50**:944–53.
- Bedford RE, Bonnier G, Maas H, Pavese F. Recommended values of temperature on the International Temperature Scale of 1990 for a selected set of secondary reference points. *Metrologia* 1996;**33**:133–54.
- Yamada T, Yoshimura M, Somiya S. Reinvestigation of the solidification point of CaO by digital pyrometry. *J Am Ceram Soc* 1986;**69**:C243–5.
- Noguchi T, Mizuno M, Conn WM. Fundamental research in refractory systems with a solar furnace-ZrO<sub>2</sub>–CaO system. *Solar Energy* 1967;**11**:145–52.
- Panek Z. Melting temperatures of MgO and CaO. *Silikaty (Prague)* 1979;**23**(2):97–102.
- Shevchenko V, Lopato LM, Stegny AI, Gerasimyuk GI, Dvernyakov VS, Pasichnyi VV. Liquidus of the HfO<sub>2</sub>–MgO and HfO<sub>2</sub>–CaO systems. *Dokl Akad Nauk SSSR, Ser A* 1979;**8**:682–5.
- Foex M. Measurement of the solidification points of several refractory oxides. *Solar Energy* 1965;**9**:61–7.
- Hlaváč J. Melting temperatures of refractory oxides. *Pure Appl Chem* 1982;**54**:681–8.
- Chase Jr MW. NIST-JANAF Thermochemical Tables, Fourth Edition, Part I. *J Phys Chem Ref Data* 1998;Monograph No. **9**:729–32.
- Wriedt HA. The Ca–O system. *Bull Alloy Phase Diagr* 1985;**6**:337–42.
- Pelton AD, Blander M. Thermodynamic analysis of ordered liquid solutions by a modified quasi-chemical approach – application to silicate slags. *Metall Mater Trans B* 1986;**17B**:805–15.
- Wu P, Eriksson G, Pelton AD. Critical evaluation and optimization of the thermodynamic properties and phase diagrams of the CaO–FeO, CaO–MgO, CaO–MnO, FeO–MgO, FeO–MnO and MgO–MnO systems. *J Am Ceram Soc* 1993;**76**:2065–75.
- Jerebtsov DA, Mikhailov GG. Phase diagram of CaO–Al<sub>2</sub>O<sub>3</sub> system. *Ceram Int* 2001;**27**:25–8.
- Zaitsev AI, Mogutnov BM. Thermodynamics of the Ca–CaO–CaF<sub>2</sub> system. *Metall Mater Trans B* 2001;**32**:305–11.
- Lindberg D, Chartrand P. Thermodynamic evaluation and optimization of the (Ca + C + O + S) system. *J Chem Thermodyn* 2009;**41**:1111–24.
- Hillert M, Wang X. Thermodynamic calculation of the CaO–MgO system. *CALPHAD* 1989;**13**:267–71.
- Hillert M, Sundman B, Wang X. An assessment of the CaO–SiO<sub>2</sub> system. *Metall Trans B* 1990;**21B**:303–12.
- Huang W, Hillert M, Wang X. Thermodynamic assessment of the CaO–MgO–SiO<sub>2</sub> system. *Metall Mater Trans A* 1995;**26A**:2293–309.
- Hallstedt B. Assessment of the CaO–Al<sub>2</sub>O<sub>3</sub> system. *J Am Ceram Soc* 1990;**73**:15–23.
- Yu H, Cheng Q, Jin Z. Thermodynamic assessment of the CaO–B<sub>2</sub>O<sub>3</sub> system. *CALPHAD* 1999;**23**:101–11.
- DeWitt DP, Richmond JC. Thermal radiative properties of materials. In: DeWitt DP, Nutter GD, editors. *Theory and practice of radiation thermometry*. New York: Wiley; 1988.
- Sokolov VA. Calcoluminescence. *Usp Fiz Nauk* 1952;**47**:538–60 [in Russian].
- Kubarev VV. Features of the drummond light of calcium dioxide. *Opt Spectrosc* 2009;**106**:242–7.
- Bevan DJM, Richardson FD. The solution of lime and liquid calcium. In: *Proceedings of the Australian Atomic Energy Symposium on the Peaceful Uses of Atomic Energy*, Australian Atomic Energy Commission. 1958. p. 586–7.
- Manara D, Sheindlin M, Heinz W, Ronchi C. High-temperature phase transition measurements in highly volatile refractory materials via laser surface heating techniques. *Rev Sci Instrum* 2008;**79**:113901–8.
- Böhler R, Welland MJ, De Bruycker F, Boboridis K, Janssen A, Eloirdi R, et al. Revisiting the melting temperature of NpO<sub>2</sub> and the challenges associated with high temperature actinide compound measurements. *J Appl Phys* 2012;**111**:113501–8.
- Preston-Thomas H. The International Temperature Scale of 1990 (ITS-90). *Metrologia* 1990;**27**:3–10.
- Preston-Thomas H. Erratum: The International Temperature Scale of 1990 (ITS-90). *Metrologia* 1990;**27**:107.
- Neuer G, Fiessler L, Groll M, Schreiber E. Critical analysis of the different methods of multiwavelength pyrometry. In: Schooley JF, editor. *Temperature: its measurement and control in science and industry*, vol. 6. New York: AIP; 1992. p. 787–9.
- Dadsetani M, Beiranvand R. Optical properties of alkaline-earth metal oxides from first principles. *Solid State Sci* 2009;**11**:2099–105.
- Manara D, Ronchi C, Sheindlin M, Lewis M, Brykin M. Melting of stoichiometric and hyperstoichiometric uranium dioxide. *J Nucl Mater* 2005;**342**:148–63.
- Sancier KM, Schott DJ, Wise H. Luminescence of solids excited by surface recombination of atoms. IV. Mechanisms of excitation and luminescence. *J Chem Phys* 1965;**42**:1233–9.
- Henderson B, Stokowski SE, Ensign TC. Luminescence from F centers in calcium oxide. *Phys Rev* 1969;**183**:826–31.
- Henderson B, Chen Y, Sibley WA. Temperature dependence of luminescence of F<sup>+</sup> and F centers in CaO. *Phys Rev B* 1972;**6**:4060–8.
- Bates JB, Wood RF. Luminescence spectrum of the F-center in CaO. *Phys Lett* 1974;**49A**:389–90.
- Bates JB, Wood RF. High-temperature luminescence spectra from F-centers in CaO. *Solid State Commun* 1975;**17**:201–3.
- Feldott J, Summers GP. Photoconductivity and luminescence of electron irradiated CaO. *Phys Rev B* 1977;**16**:1722–9.
- Park JL, Chen Y, Williams GP, Williams RT, Pogatshnik GJ. Luminescence of F<sup>+</sup> centers in CaO crystals under pulsed-laser excitation. *Phys Rev B* 1991;**43**:11991–8.
- Carrasco J, Sousa C, Illas F, Sushko PV, Shluger AL. Optical absorption and luminescence energies of F centers in CaO from ab-initio embedded cluster calculations. *J Chem Phys* 2006;**125**:1010747–9.
- Rieder KH, Weinstein BA, Cardona M, Bilz H. Measurement and comparative analysis of the second-order Raman spectra of the alkaline-earth oxides with a NaCl structure. *Phys Rev B* 1973;**8**:4780–6.
- Padanyi ZV. The Raman spectrum of Ca(OH)<sub>2</sub>. *Solid State Commun* 1970;**8**:541–3.
- Halsted PE, Moore AE. The thermal dissociation of calcium hydroxide. *J Chem Soc* 1957;**769**:3873–5.
- Ronchi C, Sheindlin M. Melting point of MgO. *J Appl Phys* 2001;**90**:3325–31.
- Zinkevich M, Djurovic D, Aldinger F. Thermodynamic modelling of the cerium–oxygen system. *Solid State Ionics* 2006;**177**:989–1000.

49. De Bruycker F, Boboridis K, Manara D, Poeml P, Rini M, Konings RJM. Reassessing the melting point of plutonium dioxide. *Mater Today* 2010;13–11:52–5.
50. Ronchi C, Iosilevski I, Yakub ES. *Equation of state of uranium dioxide*. Berlin: Springer-Verlag; 2004.
51. Guéneau C, Dupin N, Sundman B, Martial C, Dumas J-C, Gossé S, et al. Thermodynamic modelling of advanced oxide and carbide nuclear fuels: description of the U–Pu–O–C system. *J Nucl Mater* 2011;419: 145–67.
52. De Bruycker F, Boboridis K, Konings RJM, Rini M, Eloirdi R, Guéneau C, et al. On the melting behaviour of uranium/plutonium mixed dioxides with high-Pu content: a laser heating study. *J Nucl Mater* 2011;419: 186–93.